Effects of unique ion chemistry on thin-film growth by plasma–surface interactions

Muthu B. J. Wijesundara[†], **Luke Hanley**[†‡], **Boris Ni**[§], **and Susan B. Sinnott**[§]

[†]Department of Chemistry, m/c 111, University of Illinois at Chicago, 845 West Taylor Street, 4500 SES, Chicago, IL 60607-7061; and [§]Department of Chemical and Materials Engineering, University of Kentucky, 177 Anderson Hall, Lexington, KY 40506-0046

Communicated by John T. Yates, Jr., University of Pittsburgh, Pittsburgh, PA, November 8, 1999 (received for review June 14, 1999)

Plasma processing is a standard industrial method for the modification of material surfaces and the deposition of thin films. Polyatomic ions and neutrals larger than a triatomic play a critical role in plasma-induced surface chemistry, especially in the deposition of polymeric films from fluorocarbon plasmas. In this paper, low energy CF_3^+ and $C_3F_5^+$ ions are used to modify a polystyrene surface. Experimental and computational studies are combined to quantify the effect of the unique chemistry and structure of the incident ions on the result of ion-polymer collisions. $C_3F_5^+$ ions are more effective at growing films than CF_3^+, both at similar energy/atom of ≈6 eV/atom and similar total kinetic energies of 25 and 50 eV. The composition of the films grown experimentally also varies with both the structure and kinetic energy of the incident ion. Both $C_3F_5^+$ and CF_3^+ should be thought of as covalently bound polyatomic precursors or fragments that can react and become incorporated within the polystyrene surface, rather than merely donating F atoms. The size and structure of the ions affect polymer film formation via differing chemical structure, reactivity, sticking probabilities, and energy transfer to the surface. The different reactivity of these two ions with the polymer surface supports the argument that larger species contribute to the deposition of polymeric films from fluorocarbon plasmas. These results indicate that complete understanding and accurate computer modeling of plasma–surface modification requires accurate measurement of the identities, number densities, and kinetic energies of higher mass ions and energetic neutrals.

Plasma processing is a standard industrial method for the modification of material surfaces and the deposition of thin films. Plasma processing is used to produce biocompatible surfaces for tissue culture plates, contact lenses, medical implants, and other biomedical devices; photoresists for semiconductor lithography; optical coatings; polymer films for packaging and adhesives; semipermeable membranes; and chemical sensors (1–6). The modification of polymers and silicon surfaces by fluorocarbon plasmas has been particularly well studied from both practical and fundamental standpoints (1, 7–13). For example, fluoropolymers deposited from plasmas have been examined for use as diffusion barriers in drug delivery systems and vascular implant devices that resist protein fouling (6, 14). Fluorocarbon plasmas are also widely used in reactive ion etching of silicon-based semiconductor devices, in which a critical step is the growth of a protective fluoropolymer film (9, 10) (Sematech's The National Roadmap for Semiconductor Technology, http://www.sematech.org/public/home.htm). The final market value of plasma processed devices is immense, with continued growth expected. The increasing popularity of plasma processing is attributable to its experimental flexibility, the wide range of surface properties that it can impart, and the environmental advantages of this solvent-free method.

Despite its widespread usage, there are reproducibility and control problems in the practical implementation of plasma processing (6, 15). Efforts to understand the fundamental physical properties that govern plasmas seek to determine their surface modification capabilities under specific experimental conditions (1, 9–11). Accurate computer modeling of plasmas requires identification, quantification, and determination of the surface activity of the species in the plasma (16). These plasma species include atoms, atomic ions, electrons, vacuum ultraviolet photons, polyatomic ions, and radicals (6, 17). The ions and neutrals have kinetic energies ranging from thermal up to tens of electronvolts (18). They are generated by electron impact of the polyatomic feedgas, gas phase polymerization, and interactions with the substrate and reactor walls.

Polyatomic ions and neutrals larger than a triatomic play a critical role in plasma-induced surface chemistry, especially in the deposition of polymeric films from fluorocarbon plasmas (12, 13, 19, 20). However, larger polyatomics are difficult to distinguish or even detect by plasma imaging methods, and their surface chemistry is poorly understood (21). The component of plasma–surface modification caused by energetic polyatomics can be examined by using ion beams of specific mass, kinetic energy, and fluence incident on well defined surfaces (22). The specificity of polyatomic ion beams, the highly surface selective nature of the polyatomic–surface interaction, the unique collision dynamics, and the ability to transfer intact chemical functionality to the surface provide polyatomic ions with several advantages for practical surface modification (23). Atomistic simulations are valuable tools for providing information about the mechanisms responsible for the surface modification. Many of the important events take place within a few picoseconds, which makes ion-surface collisions well suited for study with molecular dynamics (MD) simulations. Several groups have used MD simulations to better understand the impact of single-atom and polyatomic ions with metal and semiconductor crystalline materials (24–31), amorphous solids (32, 33), and polymers (34). These simulations provide insight into the relationship between the physical results of the collisions and the reaction conditions, such as the mass, kinetic energy, and incident angle of the ion.

In this paper, CF_3^+ and $C_3F_5^+$ ions are used to modify a polystyrene (PS) surface. PS is chosen because it is a simple polymer surface that has been used in several plasma–surface studies (7, 35, 36). Experimental and computational studies are combined to quantify the effect of the unique chemistry and structure of the incident ions on the result of ion-polymer collisions. The different reactivity of these two ions with the polymer surface supports the argument that larger species contribute to the deposition of polymeric films from fluorocarbon plasmas.

CHEMISTRY

Materials and Methods

PS films were prepared by spin coating onto 2.5-cm-diameter stainless steel disks from 0.3% (wt/vol) PS solution in CH_2Cl_2. Survey x-ray photoelectron spectroscopy (XPS) (not shown) confirmed that the polymer film is uniformly thicker than the

Abbreviations: MD, molecular dynamics; PS, polystyrene; XPS, x-ray photoelectron spectroscopy.

[‡]To whom reprint requests should be addressed. E-mail: lhanley@uic.edu.

The publication costs of this article were defrayed in part by page charge payment. This article must therefore be hereby marked "*advertisement*" in accordance with 18 U.S.C. §1734 solely to indicate this fact.

XPS sampling depth by noting the absence of substrate signal. The absence of surface contaminants was verified by observation of a 5.5% $\pi \rightarrow \pi^*$ peak intensity at ~292 eV and a valence band spectra that are both in agreement with the literature (36).

The apparatus used for ion bombardment has been described elsewhere (37). CF_3^+ and $C_3F_5^+$ ions were formed by 80-eV electron impact ionization of C_3F_6 gas, mass-selected by a Wien filter, then transmitted by ion optics onto the PS surface at normal incidence with kinetic energies of 25 and 50 eV. Typical ion currents were 15–20 nA, and ion fluences were equivalent to 1.5×10^{16} F atoms/cm^2. A low energy electron gun was used to neutralize charge buildup on the PS surface during ion exposure. The chamber pressure during ion exposure was 10^{-7} torr, with >95% of the background gas pressure caused by C_3F_6 gas from the ion source. Control experiments found no modification to PS from the C_3F_6 background gas, or the neutralizing electron beam during ion bombardment. Samples were transferred *in situ* to the XPS chamber after ion exposure.

XPS were recorded by using a monochromatic AlK_α x-ray source (15 kV, 25 mA emission current) and a 150-mm concentric hemispherical analyzer with multichannel detector, operated at constant energy analyzer mode with a pass energy of 22 eV. The photoemission angle was normal to the surface. The data acquisition time was up to 2 hours, during which no x-ray damage to the film was observed. The main line of polystyrene was assigned to 285.0 eV of the untreated polystyrene. Peak area analysis was performed by using data analysis software of the XPS with Shirley type background correction and 35:65 Lorentzian/Gaussian product line shapes of variable widths. The C(1s) and F(1s) peak areas were converted to the atomic concentration percentages by using elemental sensitivity factors and the transmission function for the analyzer.

The computational work consisted of MD simulations of the impact of comparable hydrocarbon ions on PS at similar incident kinetic energies. To implement the simulations, Newton's equations of motion were integrated with a third-order Nordsieck predictor corrector (38), and the atoms in the system were allowed to move in time in response to the applied forces (timesteps of 0.2 fs were used). The potential used to calculate the short-range interatomic forces is the reactive empirical-bond order potential for hydrocarbons as originally parameterized by Brenner (39) and expanded and improved within the last few years. In addition, it contains long-range van der Waals interactions in the form of a Lennard–Jones potential (38) that is active only at distances greater than the covalent bond lengths. As expected, there are occasions (40) in which this potential yields reaction rates that do not agree exactly with experimental values and effects from orbital resonance and electronic excitations are not included. However, it has been successfully used to obtain insight into a variety of processes, such as cluster–surface collisions (41–43) and the chemical vapor deposition of diamond (44, 45).

The PS surfaces used in the simulations contain nine layers for a total depth of 50 Å. The bottom-most layer is held rigid throughout the simulation. The next layer from the bottom (thickness of 0.5 Å), and the same thickness from the slab edges, have Langevin frictional forces (38) applied. This maintains the surface temperature at 300 K and mimics the heat dissipation properties of a real surface. The rest of the atoms in the system (surface and ion) do not have any constraints placed on them and are designated as "active." The impacting CH_3^+ and $C_3H_5^+$ species collided at different locations within the active zone of the surface at normal incidence with external energies of 20 and 50 eV. Each trajectory was performed 40 times, and the simulations ran from 0.4 to 1.2 ps before it was determined that the result was not going to change.

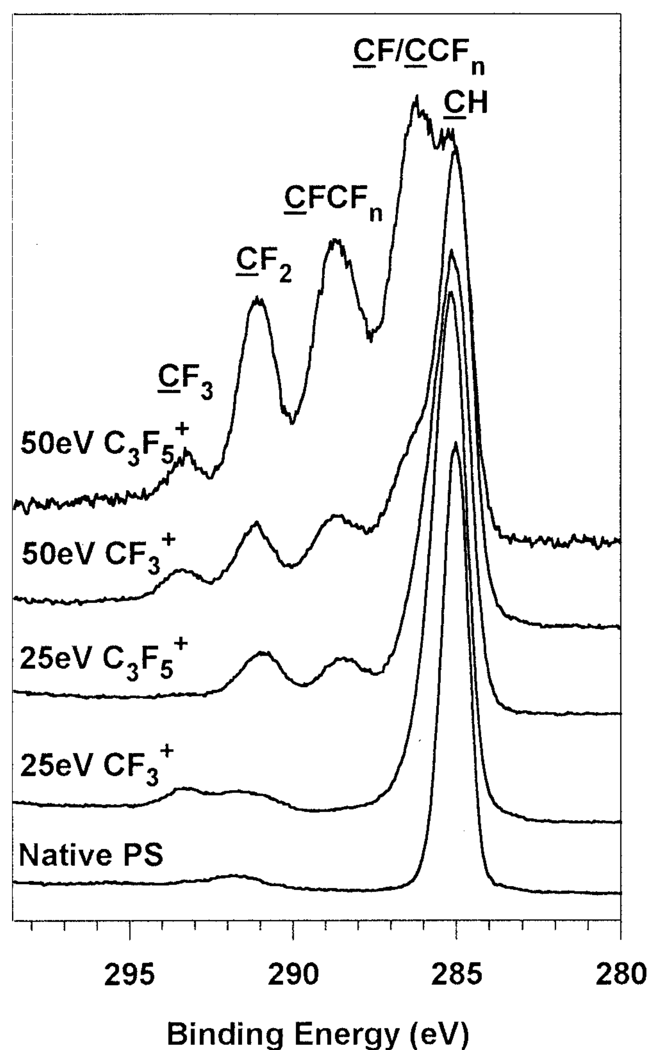

Fig. 1. C(1s) region of x-ray photoelectron spectra of native polystyrene (PS) thin film (bottom), 25-eV CF_3^+ modified PS, 25-eV $C_3F_5^+$ modified PS, 50-eV CF_3^+ modified PS, and 50-eV $C_3F_5^+$ modified PS (top). Components of C(1s) peak are labeled, with detected carbon atom underlined. All ion fluences are equivalent to 1.5×10^{16} F atoms/cm^2.

Experimental Results

Fig. 1 displays the C(1s) region of the XPS of unmodified PS (bottom trace) and PS exposed to 25-eV CF_3^+, 25-eV $C_3F_5^+$, 50-eV CF_3^+, and 50-eV $C_3F_5^+$ (top). Visual examination of Fig. 1 provides clear evidence that the surface chemistry depends on both the incident ion structure and kinetic energy. The following peak assignments are made for the C(1s) peak: CH_n (aliphatic/aromatic) at 285.0 eV (0.95 eV FWHM), CF and $\mathit{C}CF_n$ at 286.2 eV (1.9 eV), $\mathit{C}FCF_n$ at 288.7 eV (1.8eV), $\mathit{C}F_2$ at 291.1 eV (1.4 eV), $\mathit{C}F_3$ at 293.3 eV (1.4 eV), and $\pi \rightarrow \pi^*$ at 291.8 eV. These C(1s) peak assignments and widths are in absolute and relative agreement with previous data and *ab initio* calculations (8, 14, 23, 37, 46). However, the 286.2-eV peak for 25-eV CF_3^+ modified PS is fit with a narrower FWHM of 1.2 eV, because this component is attributable mostly to $\mathit{C}CF_n$ (see below), and *ab initio* calculations indicate a different peak shift than for CF (46). CH, $\mathit{C}CF_n$, CF, $\mathit{C}FCF_n$, CF_2, and CF_3 components are observed for all ion exposed PS spectra, but their relative intensities vary dramatically. The 25-eV results are particularly striking: CF_3^+ shows little $\mathit{C}FCF_n$ but pronounced CF_3 whereas $C_3F_5^+$ shows no

Table 1. Deconvolution of C(1s) XPS peak components for polystyrene exposed to 25- and 50-eV CF_3^+ and $C_3F_5^+$

Component	Binding energy, eV	25-eV CF_3^+, %	25-eV $C_3F_5^+$, %	50-eV CF_3^+, %	50-eV $C_3F_5^+$, %
CH	285.0	73	54	38	12
CF/<u>C</u>CF_n	286.2	20	31	33	42
<u>C</u>FCF_n	288.7	0.2	8	15	26
CF_2	291.1	3	7	10	16
CF_3	293.3	4	0	4	4
Atomic percent of C bound α or β to F, from C(1s)		27	46	62	88
F atomic percent from corrected F(1s)/C(1s) ratio		30	40	54	59

All ion fluences equivalent to 1.5×10^{16} F atoms/cm^2. Shown are averages of ion modified data in Fig. 1 and one replicate set of each data.

CF_3 but pronounced *C*FCF_n. Determination of percentages of each component is accomplished by peak deconvolution, and the results are displayed in Table 1.

The fluorination of PS is up to three times as efficient for $C_3F_5^+$ than for CF_3^+ when either the total kinetic energy or the nearly constant ~6-eV/atom incident ion energy are compared (using ion exposures of equivalent F atom fluence). Higher ion energy always increases the degree of fluorination for a given ion. These trends are supported both when fluorination is measured as percentage of fluorinated carbon [carbon atoms bound either α or β to F atoms, determined by deconvolution of the C(1s) components] or percentage of atomic fluorine [determined by comparison of the total F(1s) and C(1s) peak areas]. The percentages of fluorinated carbons and fluorine are lowest for 25-eV CF_3^+ (27 and 30%, respectively) and highest for 50-eV $C_3F_5^+$ (88 and 59%, respectively).

The ratio of fluorinated carbon to fluorine are lowest for 25-eV CF_3^+ at 0.9 and highest for 50-eV $C_3F_5^+$ at 1.5, indicating a difference in film chemistry or structure. More detailed information on the surface chemistry of these energetic fluorocarbon ions is obtained by quantitative analysis of the individual C(1s) components in Fig. 1 (see Table 1). The higher fluorination of PS by $C_3F_5^+$ is not attributable to CF_3 components on the surface because 25-eV $C_3F_5^+$ exposure does not form any CF_3 on the fluoropolymer film and the CF_3 contribution is constant at 4% for the other three ion exposures. Rather, the higher fluorination by $C_3F_5^+$ compared with CF_3^+ at either energy is caused by enhanced contributions from CF_2, CF, *C*FCF_n, and *C*CF_n components by the larger ion. Surface chemical differences can also be detected in a given ion when its collision energy is changed: the higher percentages of CF_2 and *C*FCF_n for 50- vs. 25-eV CF_3^+ exposure indicates that CF_3^+ ion fragments more on surface collision at the higher energy. Analogously, the appearance of CF_3 at 50 eV is attributable to fragmentation of $C_3F_5^+$ that was not predominant at 25 eV. The 286.2-eV peak for 25-eV CF_3^+ is attributable mostly to C atoms β to F atoms (*C*CF_n) whereas a majority of this peak is attributed to CF at 50 eV. Furthermore, the 291.1-eV peak for 25-eV CF_3^+ may actually be attributable in large part to the intact $\pi \rightarrow \pi^*$ component rather than CF_2, further supporting the absence of CF_3^+ fragmentation at 25 eV (see below).

The absence of F(1s) $\pi \rightarrow \pi^*$ shake-up feature (data not shown) indicates either that most of the covalently bonded F atoms are too distant from the aromatic group for the wave function overlap to occur or that the fluorine atom attachment directly or immediately adjacent to the aromatic ring does not constitute the dominant bonding environment (47). The contribution of the $\pi \rightarrow \pi^*$ shake-up satellite to the C(1s) feature will decrease with ion exposure caused by damage to the aromatic ring and the formation of saturated carbon bonding environments on the surface (7). However, the overlap of the CF_3 and CF_2 peaks prevents accurate quantification of the $\pi \rightarrow \pi^*$ peak after ion exposure, and the latter was not taken into account during C(1s) peak deconvolution of ion exposed spectra. Neglecting the $\pi \rightarrow \pi^*$ introduces an additional error of a few percent to the XPS peak areas, similar in magnitude to the peak deconvolution error.

Table 2. Results from molecular dynamics simulations of impact of CH_3^+ and $C_3H_5^+$ with polystyrene at incident kinetic energies of 20 and 50 eV per ion

	20 eV		50 eV	
	CH_3^+	$C_3H_3^+$	CH_3^+	$C_3H_5^+$
Simple scattering from the surface	12.5	22.5		2.5
Scattering from the surface with a captured H atom	7.5	5		
Knocking out H from surface	12.5		5	12.5
Adsorption on or close to surface	12.5	15	2.5	2.5
Penetration and incorporation within surface	55	57.5	17.5	17.5
Dissociation (loosing one or more H atoms)			75	25
Dissociation $CH_2 + C_2H_3$				25
Dissociation $CH + H + C_2H_3$				5
Dissociation $2CH_2 + CH$				2.5
Dissociation $CH_3 + C_2H_2$				2.5
Dissociation $CH_2 + H + C_2H_2$				5

The table shows the percentage of each process that occurs on impact.

Simulation Results

Table 2 summarizes the results obtained from the MD simulations. At 50 eV, the $C_3H_5^+$ fragments into new C_xH_y pieces 65% of the time, and the large pieces embed themselves into the PS surface. Fig. 2 displays a snapshot from a representative simulation of 50 eV $C_3H_5^+$ impacting with PS: $C_3H_5^+$ dissociates into $C_2H_2 + CH_2 + H$ fragments that are contained within the near surface region of the PS. The data in Table 2 additionally indicates that $C_3H_5^+$ adsorbs on or penetrates the surface over 32% of the time, sometimes knocking out surface hydrogen atoms to do so. Simple scattering away from the PS only occurs ~2% of the time. In contrast, at 20 eV, the CH_3^+ scatters away from the surface 20% of the time, sometimes taking a surface hydrogen atom with it. It adsorbs on or imbeds itself within the PS the rest of the time, but no fragmentation of the ion is predicted. Therefore, despite the fact that the energy/atom is nearly the same for these two processes, the results are very different and depend on the composition of the incident species.

At 20 eV, $C_3H_5^+$ scatters away from the surface in over 27% of the trajectories. The rest of the time it either adsorbs on or imbeds itself within the PS with no dissociation. Thus, at the same incident energy of 20 eV, CH_3^+ and $C_3H_5^+$ do show similar distributions of scattering and penetration. Comparison of the behavior of CH_3^+ and $C_3H_5^+$ at 50 eV shows that the CH_3^+ fragments into CH_x + 3-xH 75% of the time, a percentage that is close to the 65% overall dissociation rate for $C_3H_5^+$ at this energy. Examination of the details of dissociation in Table 2,

CHEMISTRY

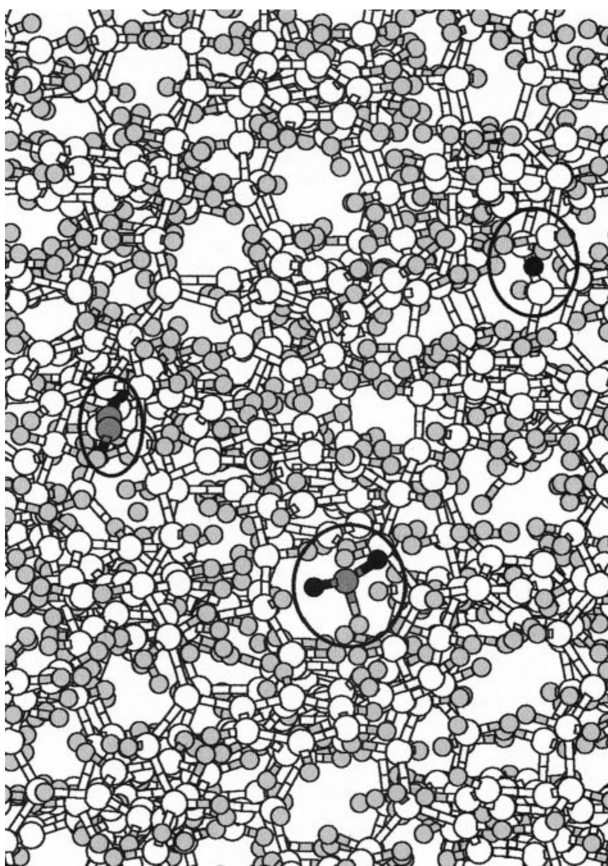

Fig. 2. A snapshot from a MD simulation of $C_3H_5^+$ impacting polystyrene with an incident energy of 50 eV. The result of this collision is the dissociation of the $C_3H_5^+$ into C_2H_2 + CH_2 + H fragments that are contained within the polystyrene. There is little change in the structure of the polystyrene surface aside from the incorporation of these fragments. White and light-gray spheres represent surface carbon and hydrogen atoms, respectively. Dark-gray and black spheres represent $C_3H_5^+$ carbon and hydrogen, respectively. The view is from the top of the surface.

however, shows that the larger $C_3H_5^+$ ion dissociates into many more species than does the smaller CH_3^+ ion.

In all of the simulation trajectories, the ions transfer the majority of their external (incident) energy to the surface, with the exact amount depending on the incident ion, external energy, and the outcome of the collision. For instance, when the CH_3^+ ion impacts at 20 eV and scatters away, ~84% of the energy is transferred to (and dissipated by) the PS. About 11% is unchanged as ion kinetic energy, and ~5% is transformed into ion internal energy (manifest as vibrations and rotations). In contrast, when the $C_3H_5^+$ ion impacts at 20 eV and scatters away, 95% of the energy is transferred to the surface whereas only 2% remains as ion kinetic energy and 3% is transformed into internal ion energy. However, when the collision outcome is ion incorporation within the surface, there is much less difference between the outcomes for the CH_3^+ and $C_3H_5^+$ ions, with 97–98% of the incident kinetic energy transferred to the PS and 2–3% transformed into internal ion energy. At incident energies of 50 eV, the CH_3^+ is always incorporated within the PS. About 97% of the incident ion energy is transferred to the surface when the ion fragments into CH_2 + H whereas over 99% is transferred to the PS when the ion is incorporated with no fragmentation. For $C_3H_5^+$ at 50 eV, the energy transfers depend slightly on the decay mechanisms. For instance, when the ion fragments into C_3H_n + 5-nH, 5% of the energy is transformed into internal energy and 94% is transferred to the surface. However, when the ion fragments into C_2H_3 + CH_2, only 1% is in internal energy and 99% is transferred to the surface.

Discussion and Conclusions

Despite the fact that the experiments and simulations do not examine exactly the same systems, there is excellent agreement with regard to the observed trends in behavior with ion size and relative incident energy. For instance, both the experiments and simulations clearly show that $C_3F_5^+$ or $C_3H_5^+$ ions are up to three times more effective at growing films than CF_3^+ or CH_3^+, when compared at both similar total ion kinetic energy and similar energy/atom (~6 eV/atom). The composition of the films grown experimentally also varies with the two ions because of higher fractions of CF_2, CF, *C*FCF_n, and *C*CF_n for $C_3F_5^+$. Both $C_3F_5^+$ and CF_3^+ should be thought of as covalently bound polyatomic precursors or fragments that can react and become incorporated within the PS surface, rather than merely donating F atoms. Direct deposition of intact $C_3F_5^+$ occurs while preserving at least a portion of the gas phase structure $CF_2CF{=}CF_2^+$ (48), especially at 25 eV. Most of the CF_3^+ ions are also deposited intact onto the PS surface at 25 eV. However, CF_3^+ displays significant dissociation and higher fluorination at 50 eV collisions. Low energy polyatomic ions have been previously covalently bound to organic surfaces, but ions of similar stoichiometry were not compared (23, 49), and the percentages of surfaces species were not quantified (49).

The simulations provide additional details about the relative frequency of simple scattering, dissociation, and incorporation of the hydrocarbon analogs of CF_3^+ and $C_3F_5^+$. They also illustrate the more complex dissociation behavior exhibited by the larger ion that can influence the way in which the film grows by controlling the type and reactivity of the precursors. It is well established that energy transfer to the surface by polyatomic ions can be very efficient and depends on ion and surface structure (50, 51). The simulations support these observations but also demonstrate that energy transfer differs between the scattering and deposition processes. The overall behavior of the fluorocarbon and hydrocarbons should be similar, as their bond energies are close in value and their known chemical behaviors are alike (52). However, there are some differences. For instance, F that has been knocked loose on impact is more likely than H to react with the hydrogen within the PS surface (HF has a bond dissociation energy that is ~31 kcal/mol higher than H_2) (52). This could influence the growth so that analogously deposited hydrocarbon films could have morphologies that differ from the fluorocarbon films.

Furthermore, the simulations model the impact of a single ion on a pristine PS surface whereas the experiments examine a surface that has been modified by multiple ion–surface collisions. The PS is therefore undergoing continuous change from the initial PS surface during the course of the experiment: the use of hydrocarbon projectiles in the simulation partially takes this effect into account by avoiding the introduction of new elements to the surface during ion bombardment. However, ongoing work is examining the film growth as a function of ion dose. Despite these limitations, both simulations and experiments show that the behavior of the incident ions on impact will depend on more than just the incident kinetic energy or energy per atom.

These results on ion–polymer surface modification are highly relevant to the formation of polymer films from fluorocarbon plasmas (the competitive process of surface etching is not considered here, nor are the effects of substrate on polymerization). CF_x (especially CF_2) radicals generated in fluorocarbon plasmas have been considered the dominant precursors to polymer film formation (11, 53–55). Ions emanating from the plasma also play a critical role in polymerization (55, 56).

However, only the role of atomic and CF_x^+ ions have been extensively studied (22, 56). Furthermore, the kinetic energy of the ions rather than their chemical composition has often been considered most critical (9). However, recent studies have observed larger $C_{x>1}F_y$ ions and radicals in fluorocarbon plasmas (13, 57). Recent work has argued that these larger $C_{x>1}F_y$ species, rather than CF_2, are the dominant precursors to polymer film formation (20). The results presented here clearly indicate at least one of these larger species, $C_3F_5^+$, can behave as a precursor to fluorocarbon film formation on a polymer surface. The size and structure of the ions do affect polymer film formation via differing chemical structure, reactivity, sticking probabilities, and energy transfer to the surface (23, 58). Although the energy of the ion is critical, a polyatomic ion does not necessarily behave as the sum of its individual atoms (56, 59). The $C_3F_5^+$ ion maintains most of its molecular character at 25 eV, although the kinetic to internal energy transfer is sufficient to fragment at least some of its C—C and/or C—F bonds at 50 eV. Polymer films grow most readily from plasma feedgases with F/C ratio less than ~2.5 (6, 10). Thus, C_3F_6 feedgases more readily grow polymer films than CF_4, C_2F_6, or C_3F_8 (19, 58). This effect is attributable in part to the higher intensities of $C_3F_5^+$ and other large, unsaturated polyatomic ions in the C_3F_6 plasma. Enhanced $C_3F_5^+$ intensities also contributes to the higher *C*F-CF_n, and CF_2 components in the C(1s) XPS of the fluorocarbon films from C_3F_6 plasma and the production of those films at higher ion energies (self-bias voltages) (58). These results indicate that complete understanding and accurate computer modeling of plasma–surface modification requires accurate measurement of the identities, number densities, and kinetic energies of higher mass ions and energetic neutrals (16). The differing reactivities of these polyatomics as a function of their kinetic energies in the plasma also must be taken into account.

The experimental work was supported by the National Science Foundation (Grants CHE-9457709, CHE-9632517, and CHE-9708922). The theoretical work was also supported by the National Science Foundation (Grants CHE-9708049 and DMR-9809686).

1. Yasuda, H. (1985) *Plasma Polymerization* (Academic, New York).
2. Gerenser, L. J. (1994) in *Plasma Surface Modification of Polymers*, eds. Strobel, M., Lyons, C. & Mittal, K. L. (VSP, Zeist, The Netherlands), pp. 43–64.
3. Kostelak, R. L., Weidman, T. W., Vaidya, S., Joubert, O., Palmateer, S. C. & Hibbs, M. (1995) *J. Vac. Sci. Technol. B* **13,** 2994–2999.
4. Shi, F. F. (1996) *J. Macromol. Sci. Rev. Macromol. Chem. Phys.* **C36,** 795–826.
5. Johnson, E. E. & Ratner, B. D. (1996) *J. Electron Spectrosc. Relat. Phenom.* **81,** 303–318.
6. Chan, C.-M., Ko, T.-M. & Hiraoka, H. (1996) *Surf. Sci. Rep.* **24,** 1–54.
7. Clark, D. T., Feast, W. J., Tweedale, P. J. & Thomas, H. R. (1980) *J. Polym. Sci. Polym. Chem. Ed.* **18,** 1651–1664.
8. Strobel, M., Corn, S., Lyons, C. S. & Korba, G. A. (1987) *J. Polym. Sci. Polym. Chem. Ed.* **25,** 1295–1307.
9. Kirmse, K. H. R., Wendt, A. E., Oehrlein, G. S. & Zhang, Y. (1994) *J. Vac. Sci. Technol. A* **12,** 1287–1292.
10. Coburn, J. W. (1994) *Appl. Phys. A* **59,** 451–458.
11. Gray, D. C., Mohindra, V. & Sawin, H. H. (1994) *J. Vac. Sci. Technol. A* **12,** 354–364.
12. Horie, M. (1995) *J. Vac. Sci. Technol. A* **13,** 2490–2497.
13. Stoffels, W. W., Stoffels, E. & Tachibana, K. (1998) *J. Vac. Sci. Technol. A* **16,** 87–95.
14. Gengenbach, T. R. & Griesser, H. J. (1998) *Surf. Interface Anal.* **26,** 498–511.
15. Poll, H.-U. & Schreiter, S. (1997) *Surf. Coat. Technol.* **93,** 105–111.
16. Graves, D. B., Kushner, M. J., Gallagher, J. W., Garscadden, A., Oehrlein, G. O. & Phelps, A. V. (1996) *Database Needs for Modeling and Simulation of Plasma Processing: Report by the Panel on Database Needs in Plasma Processing, National Research Council* (National Academic Press, Washington, DC).
17. Zalm, P. C. (1985) *Pure Appl. Chem.* **57,** 1253–1264.
18. Nichols, C. A., Woodworth, J. R. & Hamilton, T. W. (1998) *J. Vac. Sci. Technol. A* **16,** 3389–3395.
19. Leezenberg, P. B., Reiley, T. C. & Tyndall, G. W. (1999) *J. Vac. Sci. Technol. A* **17,** 275–281.
20. Cunge, G. & Booth, J. P. (1999) *J. Appl. Phys.* **85,** 3952–3959.
21. Wiesemann, K. (1996) *Pure Appl. Chem.* **68,** 1029–1034.
22. Bello, I., Chang, W. H. & Lau, W. M. (1994) *J. Vac. Sci. Technol. A* **12,** 1425–1430.
23. Ada, E. T., Kornienko, O. & Hanley, L. (1998) *J. Phys. Chem. B* **102,** 3959–3966.
24. Nakamura, M., Tsukada, M. & Aono, M. (1993) *Surf. Sci.* **283,** 46–51.
25. Webb, R. P., Smith, R., Chakarov, I. & Beardmore, K. (1996) *Nucl. Instrum. Methods Phys. Res. Sect.B* **112,** 99–104.
26. Hensel, H. & Urbassek, H. M. (1998) *Phys. Rev. B* **57,** 4756–4763.
27. Hoffman, A., Paterson, P. J. K., Johnston, S. T. & Prawer, S. (1996) *Phys. Rev. B* **53,** 1573–1578.
28. Ghaly, M. & Averback, R. S. (1994) *J. Phys. Chem. Solids* **55,** 945–953.
29. Abrams, C. F. & Graves, D. B. (1998) *J. Vac. Sci. Technol. A* **16,** 3006–3019.
30. Carter, L. E. & Carter, E. A. (1996) *J. Phys. Chem.* **100,** 873–887.
31. Helmer, B. A. & Graves, D. B. (1997) *J. Vac. Sci. Technol. A* **15,** 2252–2261.
32. Uhlmann, S., Frauenheim, T. & Lifshitz, Y. (1998) *Phys. Rev. Lett.* **81,** 641–644.
33. Koponen, I., Hautala, M. & Sievanen, O.-P. (1997) *Nucl. Instrum. Methods Phys. Res. Sect. B* **129,** 349–355.
34. Brenner, D. W., Shenderova, O. & Parker, C. B. (1997) *Proceedings of the Materials Research Society* (Mater. Res. Soc., Pittsburgh), Vol. 438, p. 491.
35. Strobel, M., Thomas, P. A. & Lyons, C. S. (1987) *J. Polym. Sci. Polym. Chem. Ed.* **25,** 3343–3348.
36. France, R. M. & Short, R. D. (1998) *Langmuir* **14,** 4827–4835.
37. Hanley, L., Lim, H., Schultz, D. G., Garbis, S., Yu, C., Ada, E. T. & Wijesundara, M. B. J. (1999) *Nucl. Instrum. Methods Phys. Res. Sect. B* **157,** 174–182.
38. Allen, M. P. & Tildesley, D. J. (1987) *Computer Simulation of Liquids* (Oxford Univ. Press, New York).
39. Brenner, D. W. (1990) *Phys. Rev. B* **42,** 9458–9471.
40. de Sainte Claire, P., Son, K., Hase, W. L. & Brenner, D. W. (1996) *J. Phys. Chem.* **100**, 1761–1766.
41. Qi, L. & Sinnott, S. B. (1997) *J. Phys. Chem. B* **101,** 6883–6890.
42. Qi, L. & Sinnott, S. B. (1998) *J. Vac. Sci. Technol. A* **16,** 1293–1296.
43. Qi, L., Young, W. L. & Sinnott, S. B. (1999) *Surf. Sci.* **426,** 83–91.
44. Alfonso, D. R. & Ulloa, S. E. (1993) *Phys. Rev. B* **48,** 12235–12239.
45. Alfonso, D. R., Ulloa, S. E. & Brenner, D. W. (1994) *Phys. Rev. B* **49,** 4948–4953.
46. Smentkowski, V. S., Yates, J. T. J., Chen, X. & Goddard, W. A. I. (1997) *Surf. Sci.* **370,** 209–231.
47. Clark, D. T. & Dilks, A. (1977) *J. Polym. Sci. Polym. Chem. Ed.* **15,** 15–30.
48. Freiser, B. S. & Beauchamp, J. L. (1974) *J. Am. Chem. Soc.* **96,** 6260–6269.
49. Wade, N., Pradeep, T., Shen, J. & Cooks, R. G. (1999) *Rapid Commun. Mass Spectrom.* **13,** 986–993.
50. Lim, H., Schultz, D. G., Gislason, E. A. & Hanley, L. (1998) *J. Phys. Chem. B* **102,** 4573–4580.
51. Koppers, W. R., Gleeson, M. A., Lourenco, J., Weeding, T. L., Los, J. & Kleyn, A. W. (1999) *J. Chem. Phys.* **110,** 2588–2596.
52. Loudon, G. M. (1984) *Organic Chemistry* (Addison–Wesley, Reading, MA).
53. Gray, D. C., Sawin, H. H. & Butterbaugh, J. W. (1991) *J. Vac. Sci. Technol. A* **9,** 779–785.
54. Mackie, N. M., Venturo, V. A. & Fisher, E. R. (1997) *J. Phys. Chem. B* **101,** 9425–9428.
55. Inayoshi, M., Ito, M., Hori, M., Goto, T. & Hiramatsu, M. (1998) *J. Vac. Sci. Technol. A* **16,** 233–238.
56. Coburn, J. W. (1994) *J. Vac. Sci. Technol. A* **12,** 1417–1424.
57. Scharzenbach, W., Cunge, G. & Booth, J. P. (1999) *J. Appl. Phys.* **85,** 7562–7568.
58. Schaepkens, M., Standaert, T. E. F. M., Rueger, N. R., Sebel, P. G. M., Oehrlein, G. S. & Cook, J. M. (1999) *J. Vac. Sci. Technol. A* **17,** 26–37.
59. Ada, E. T. & Hanley, L. (1998) *Int. J. Mass Spectrom. Ion Processes* **174,** 231–244.